Maximising Acoustoelectric Signal Strength via Optimal Bipolar Electrode Placement

Sathiyamoorthy Selladurai[1], Alec Bales-D'Cruze[1], Andy Adler[1], Nicola Schieda[2], and Carlos Rossa[1]
[1]*Dep. of Systems and Computer Engineering, Carleton University, Ottawa, ON, Canada*
[2]*Dep. of Radiology, Radiation Oncology and Medical Physics, University of Ottawa, Ottawa, ON, Canada*
selladuraisathiyamoo@carleton.ca; alecbalesdcruze@cmail.carleton.ca; adler@sce.carleton.ca; nschieda@toh.ca; carlosrossa@cunet.carleton.ca

***Abstract*—The acoustoelectric (AE) effect, i.e., the modulation of electrical impedance with ultrasound (US) waves, is a promising mechanism for combining the high spatial resolution of US with the conductivity sensitivity of electrical impedance measurements. However, the AE signal is extremely weak and difficult to measure. In this work, we present a coupled 3D simulation framework integrating the Matlab Ultrasound Toolbox (MUST) with the finite-element bioimpedance solver EIDORS to model AE signal generation in heterogeneous tissue. Using this framework, we investigate AE responses produced by both focused and plane-wave US excitations in the presence of bipolar internal electrodes. Focused US is shown to produce an AE response with significantly higher peak amplitude, while plane-wave excitation yields a more spatially distributed but lower-amplitude signal, highlighting a fundamental trade-off between sensitivity and spatial coverage. Our results also demonstrate that electrode alignment with the US propagation direction maximizes AE sensitivity. The proposed MUST-EIDORS simulation framework provides quantitative guidance for optimizing US transmission strategies and electrode configurations in minimal AE measurements. These findings support the feasibility of AE imaging and lay the groundwork for future experimental validation.**

***Index Terms*—Acoustoelectric effect, acoustoelectric tomography, ultrasound, EIDORS, MUST, FEM simulation.**

I. Introduction

Acoustoelectric tomography (AET) is a hybrid imaging modality that combines the spatial resolution of focused ultrasound (US) with the contrast of electrical impedance tomography [1]. In AET, a number of electrodes deliver an electrical current to a tissue while simultaneously measuring the induced voltage. An US wave is then propagated through the tissue. As the wave induces microscopic periods of compression and rarefaction spatially encoded at the focal point, it alters the tissue's conductivity within, proportionally to the acoustoelectric (AE) coupling constant - a phenomenon called the AE effect. These localized conductivity perturbations are detected as voltage modulations at the frequency of ultrasonic wave, providing sufficient information to infer the spatial distribution of the tissue conductivity [2]–[4].

Early studies established the feasibility of AET and demonstrated that AE signals are detectable in conductive media [3] under noise and modelling uncertainties [5]. Subsequent work expanded these concepts into current density imaging to localize bioelectric current distributions [6]–[8]. US field characteristics play a critical role in determining spatial resolution and AE signal strength, as governed by acoustic beam focusing and energy distribution properties [9]–[11]. In addition to focused ultrasound, plane-wave excitation has recently gained attention in ultrafast US imaging due to its large field-of-view, high temporal resolution. Plane waves distribute acoustic energy more uniformly, potentially enabling more robust AE signal generation when large volumes must be interrogated rapidly [12]. However, the impact of plane-wave excitation on AE signal strength and sensitivity to conductivity heterogeneity remains insufficiently studied [1], [12]–[14]. Recent advances in ultrafast ultrasound systems have further enabled high-sensitivity AE measurements with improved temporal resolution [13].

Most studies rely on a large number of surface electrodes, offering low sensitivity at deep depths. In our previous work, we proved that a single pair of internal electrodes suffices for 3D AET image reconstruction [12]. Internal electrodes can be integrated in biopsy needles and catheters to image the tissue directly from within. With only one or two pairs of internal electrodes the trade-off between focused and plane-wave US excitation becomes even more relevant. While focused US can provide higher conductivity modulation and spatial selectivity, plane-wave may offer improved robustness to electrode misalignment and positioning errors. Understanding how these two excitation strategies influence the measured AE signal is essential for optimizing minimal AET system design. However, there has been no comprehensive 3D simulation framework that integrates realistic focused/plane wave US propagation with finite-element bioimpedance modelling to enable such study. Existing work either focuses on analytical models, 2D geometries, or standalone electrical simulations without explicit coupling to the acoustic field [12], [15].

In this paper we address this gap by presenting a coupled 3D forward simulation framework that combines the Matlab Ultrasound Toolbox (MUST) for high-fidelity US field simulation [16], [17], with the Diffuse Optical Reconstruction Software (EIDORS) for finite-element bioimpedance modeling [18], [19]. We evaluate AE signal under both focused and plane-wave US excitation for different bipolar internal electrode

We acknowledge the support of the Government of Canada's New Frontiers in Research Fund (NFRF), [NFRFE-2024-00317].

Nous remercions le fonds Nouvelles frontières en recherche du gouvernement du Canada de son soutien [NFRFE-2024-00317].

configurations, using a mesh containing a spherical inclusion with varying conductivity contrast. We assess the difference in the AE signal measured in the presence and absence of an inclusion. This comparison offers insights into how electrode placement inside and outside of the inclusion affects the ability of the system to detect inclusions in the tissue, which is fundamental for AET image reconstruction. In addition, we investigate the effect of electrode separation, demonstrating that alignment with the ultrasound propagation direction yields a robust AE response that remains largely invariant to electrode spacing, whereas perpendicular configurations exhibit a rapid degradation in signal amplitude with increasing separation.

This paper is organized as follows: Section II outlines the simulation model, followed in Section III describes the simulation scenarios. Section IV analyzes the results and discusses their implications in minimal AET. Finally, Section V describes the conclusions. The contributions of this work are: 1) A coupled 3D forward model integrating MUST and EIDORS; 2) A comparative analysis of focused *vs* plane-wave US excitation and internal electrode placement for minimal AET; and 3) Quantitative analysis of AE signal sensitivity to localized conductivity heterogeneity.

II. Coupled EIDORS-MUST Simulation

The simulation setup is illustrated in Fig. 1. In EIDORS, Fig. (a), the tissue is represented as a cylindrical volume generated using *Netgen* and discretized into tetrahedral elements. A spherical inclusion of radius 2.5 mm is positioned at the centre of the mesh to represent a localized region of altered electrical properties. The mesh conductivity is set to $\sigma_0 = 1$ S/m whereas the inclusion conductivity σ_1 is set to $\sigma_1 = N\sigma_0$, where $N \in [1/8, 1/6, 1/4, 1/2, 1, 2, 4, 6, 8]$ is the contrast ratio reflecting impedance contrasts between normal and malignant tissue. When $N = 1$, the medium is homogeneous [10], [19]. Two spherical electrodes of radius 0.5 mm are symmetrically positioned at the centre of the mesh to deliver a constant electrical current $i(t)$ while measuring the induced voltage $v(t)$. The electrodes are inside and outside the inclusion by setting $e = 10$ mm or $e = 5$ mm, see Fig. 1(b). The angle of electrodes θ is varied from 0° to 180° in 10° increments.

The AE effect is modelled as a pressure-dependent conductivity modulation expressed as

$$\sigma(\mathbf{r}, t) = \sigma_0(\mathbf{r}) + k(\mathbf{r})\, p(\mathbf{r}, t), \tag{1}$$

where $\mathbf{r}$ gives the coordinates of a point within the mesh, $p(\mathbf{r}, t)$ denotes the instantaneous acoustic pressure and $k(\mathbf{r})$ is the AE coupling constant [3], [7], [12]. The background mesh is assigned $k_0 = 10^{-6}$ Pa^{-1}, which lies within the range reported for saline and biological tissues [3], [7], [20].

Ultrasound wave propagation is simulated in MUST as a 16×16 matrix array transducer having an element pitch of 300 μm, a centre frequency of 2.5 MHz, and a fractional bandwidth of 60%. The acoustic medium is assumed to be homogeneous with a speed of sound of 1540 m/s. For focused excitation, transmit delays are applied to focus the US beam at a depth of 30 mm along z. For plane-wave, no transmit delays are applied. The 3D acoustic pressure field is evaluated over a rectilinear grid spanning 14 mm laterally and 50 mm axially. The frequency-domain pressure field is converted to time domain using the inverse fast Fourier transform. US pressure fields are normalized to have the same total acoustic energy.

The time-dependent US pressure field is interpolated onto the EIDORS mesh using a grid-to-FEM mapping operator, and the resulting conductivity perturbation is applied to every element in the mesh prior to solving the electrical forward problem for each time step. A current of $i(t) = 1$ mA is applied between the electrodes, and the resulting voltage difference is computed in EIDORS.

III. Simulation Scenarios

Simulations are designed to evaluate the influence of electrode placement, orientation, conductivity contrast, and focused *vs* plane wave on the measured AE signal.

In **Scenario 1**, the electrodes are first positioned outside the inclusion with conductivity set higher than the background with $N = 4, 6, 8$. The electrodes are also positioned inside the inclusion with conductivity contrast set to $N = 2$. The electrode orientation is swept from $\theta = 0^\circ$ to 180° in 10° increments. Both focused and plane-wave US excitations are used.

In **Scenario 2**, the electrodes are inside the inclusion and focused US excitation is used. Hypoconductive and hyperconductive inclusions are simulated by setting $N = 4, 6, 8$ and $N = 1/4, 1/6, 1/8$, respectively. The electrode voltages are calculated for all scenarios, and the peak-to-peak amplitudes extracted. For each configuration above, we run an equivalent simulation in a homogeneous medium ($N = 1$). The peak-to-peak voltages between the scenarios above and the homogeneous medium are compared as a quantitative measure of sensitivity to conductivity heterogeneity.

We also investigate the influence of electrode separation in a homogeneous medium $(N = 1)$ under focused ultrasound excitation. The following two scenarios isolate the effect of electrode spacing from conductivity heterogeneity and orientation angle to quantify how the spatial overlap between the focused acoustic pressure field and the induced current density affects the measured AE signal.

In **Scenario 3** the electrodes are placed at the centre of the mesh along the ultrasound propagation direction (z-axis), corresponding to alignment with the acoustic wavefront. The inter-electrode distance e is varied from 2.5 mm to 20 mm.

In **Scenario 4** the electrodes are placed at the centre of the mesh orthogonally to the ultrasound propagation direction (along the x-axis). The electrode distance e is varied from 2.5 mm to 20 mm.

In all 4 scenarios, the AE effect is modelled using the pressure-dependent conductivity formulation in (1), and a constant current $i(t) = 1$ mA is applied between the electrodes. For each configuration, the time-domain AE voltage is computed, and the peak-to-peak amplitude is extracted.

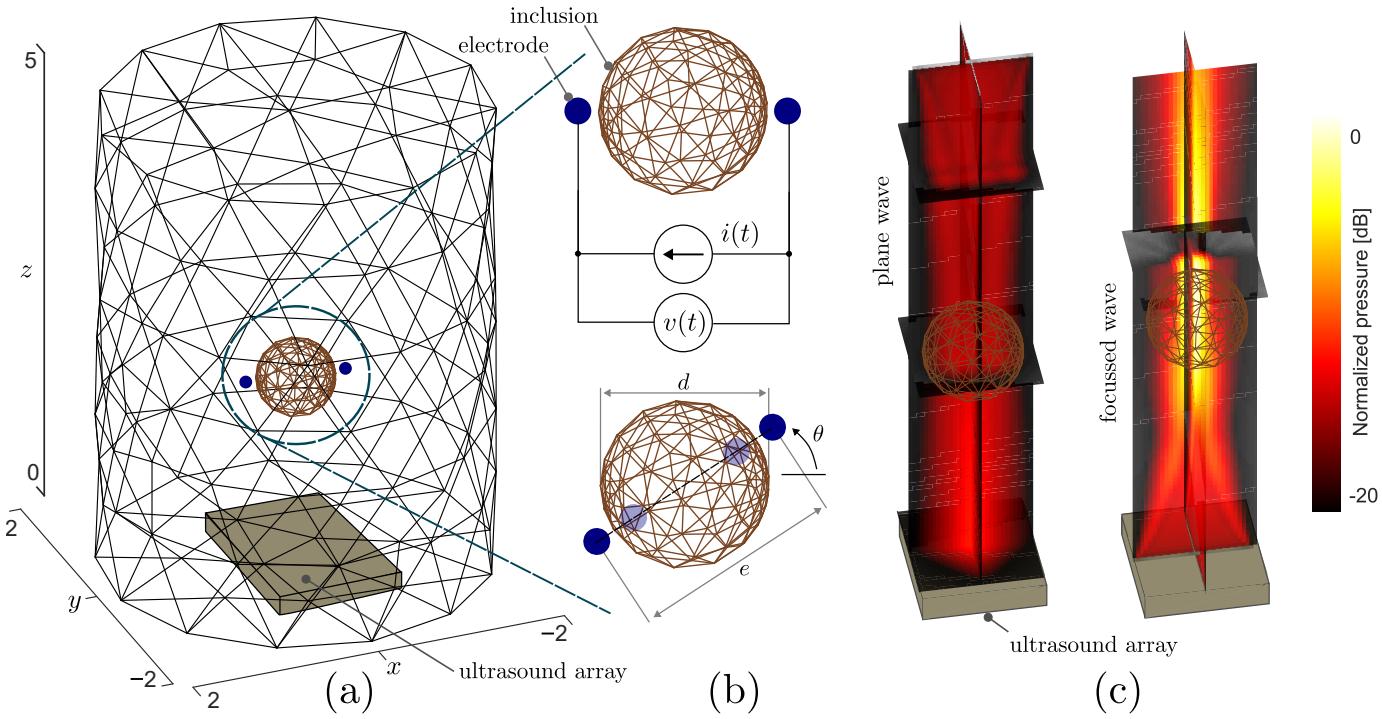

Fig. 1. Coupled MUST–EIDORS simulation. Fig. (a) 3D mesh in EIDORS representing the tissue with a spherical inclusion and two internal electrodes. A 16×16 US matrix array transmits acoustic waves along z. Fig. (b) Zoomed-in view of the bipolar electrode configuration delivering a current $i(t)$ and measuring voltage $v(t)$. The inclusion diameter is d, the distance between the electrodes is e, and θ is the electrode orientation angle relative to the xy plane. Fig. (c) shows the normalized ultrasonic pressure of plane and focused wave simulated in MUST.

IV. Results and Discussion

The first two columns of Fig. 2(a) show the AE voltages for Scenario 1 at electrode orientations $\theta = 0°$ and $\theta = 90°$ outside the spherical inclusion. Results are reported for a homogeneous medium ($N = 1$) and a heterogeneous medium ($N = 2$) under both focused and plane-wave US excitation, together with their corresponding difference signals. The third column summarizes the peak-to-peak AE voltage as a function of electrode orientation from $0°$ to $180°$.

In the homogeneous case, when the electrodes are aligned with the US propagation direction ($90°$), focused excitation produces a peak-to-peak AE voltage of approximately 118.8 μV, compared to approximately 50 μV for plane-wave excitation. At $\theta = 0°$, the peak-to-peak AE voltage is approximately 51.3 μV for focused excitation. In the heterogeneous configuration, the focused response at $90°$ reaches approximately 57.1 μV, whereas the plane-wave response is approximately 30 μV. The corresponding difference AE signal at $90°$ is approximately 51.6 μV for focused excitation and approximately 25 μV for plane-wave excitation, indicating that when electrodes are aligned with the US beam, focused US enhances sensitivity to conductivity contrast by approximately twofold relative to plane-wave excitation.

Fig. 2(b) reports the same analysis when the electrodes are inside the inclusion. At $\theta = 0°$, plane-wave excitation produces a peak-to-peak AE voltage of approximately 118.7 μV in the homogeneous case ($N = 1$), compared with approximately 41.3 μV for the heterogeneous case. At $\theta = 90°$, the homogeneous response reaches approximately 128.9 μV, while the heterogeneous response is approximately 44.3 μV. The corresponding difference AE signal at $90°$ is approximately 84.9 μV. These results demonstrate that with intralesional electrode placement, the AE response remains strongly dependent on electrode orientation, with maximum modulation observed near $\theta = 90°$.

The results in Scenario 2 are summarized in Fig. (3). For inclusions with reduced conductivity ($N = 1/4, 1/6, 1/8$), the AE peak-to-peak voltage increases as N decreases. Since the inclusion is hypoconductive, the AE amplitude in heterogeneous medium is lower than in the homogeneous case, with the largest reductions occurring near $90°$, where the focused pressure field and current density overlap most strongly with the low-conductivity region. The right panel plots the corresponding AE peak-to-peak voltage difference ΔAE between heterogeneous and homogeneous media. At $0°$, the heterogeneous AE peak-to-peak voltage is reduced by 10-30% relative to the homogeneous case as the contrast factor increases from $N = 4$ to $N = 8$, whereas at $90°$ the reduction reaches 30-50%. These results indicate that, with intralesional electrodes, hypoconductive inclusions remain detectable, with the largest signal loss near angles where the US focus and current density are most strongly concentrated within the inclusion.

When the inclusion is hyperconductive ($N = 4, 6, 8$), the AE amplitude in heterogeneous media is higher than the homogeneous case for all contrast factors and electrode

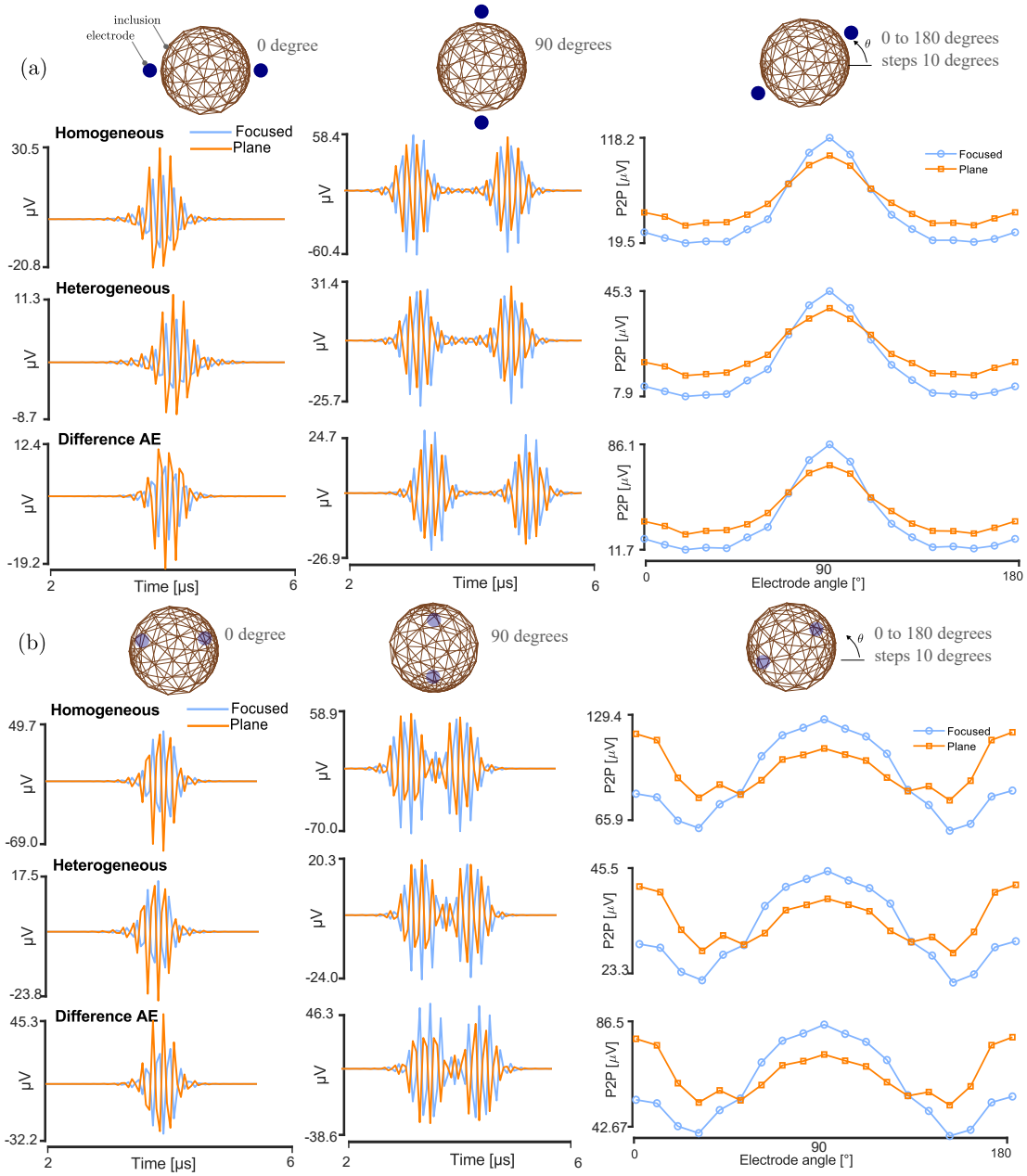

Fig. 2. AE response for focused and plane-wave US under for electrodes *outside* (a) and *inside* (b) the inclusion. Rows correspond to homogeneous tissue (top), heterogeneous tissue containing the inclusion (middle), and the difference in signal between them (bottom). Columns show time-domain AE signals for fixed electrode orientations of 0° and 90° (left and middle), and the peak-to-peak AE voltage for 0° to 180°.

angles, with the largest relative increases observed near 90°, where the focused pressure field and current density overlap with the high-conductivity region. The right panel presents the corresponding AE peak-to-peak voltage difference ΔAE between heterogeneous and homogeneous media. At 0° electrode orientation, focused excitation yields an 20-40% increase in AE peak-to-peak voltage when going from homogeneous tissue to the lowest contrast level, rising by 60-100% for the highest contrast when electrodes reside inside the hyperconductive sphere. At 90°, where the overlap between the focus, current density, and inclusion is maximal, peak-to-peak voltage increases by 80-150% as the contrast multiplier increases.

Fig. 4 presents the AE peak-to-peak voltage as a function of electrode separation in a homogeneous medium under focused ultrasound excitation in Scenarios 3 and 4. Interestingly, at very small electrode separations, the perpendicular configuration (Scenario 4) exhibits a higher AE amplitude than the parallel configuration (Scenario 3). This can be attributed to stronger lateral pressure gradients at the focal region, which enhance local coupling between the acoustic field and the current density when electrodes are closely spaced across the beam. However, the AE signal rapidly decreases as the electrode separation increases.

A clear contrast in behaviour is observed between the two configurations. In Scenario 3, the AE response remains

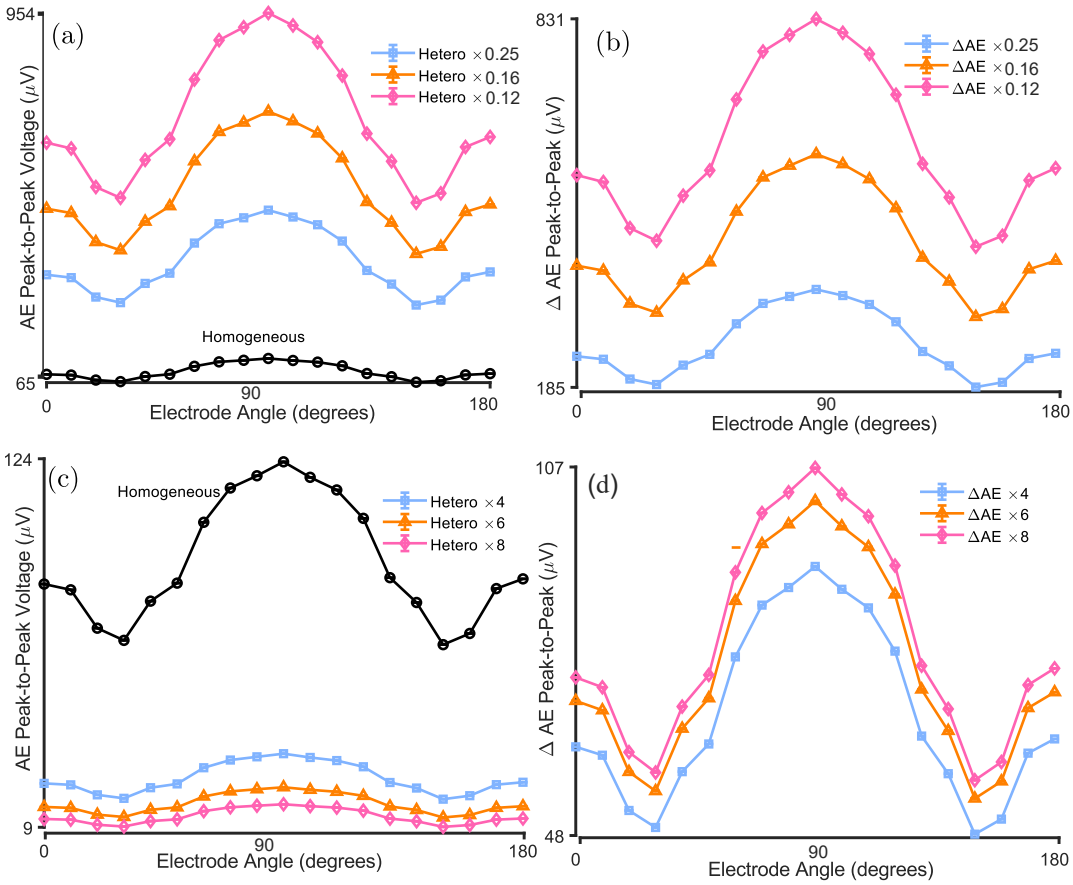

Fig. 3. AE peak-to-peak voltage for Scenario 2, with electrodes inside the inclusion under focused US. (a) AE peak-to-peak voltage as a function of electrode orientation (0° to 180°) for a homogeneous medium media with inclusions of lower conductivity ($N = 1/4,\ 1/6,\ 1/8$). (b) Peak-to-peak voltage difference (ΔAE), between the heterogeneous and homogeneous cases. (c) Peak-to-peak voltage as a function of electrode orientation for a homogeneous medium and for media with inclusions of higher conductivity ($N = 4,\ 6,\ 8$). (d) AE signal difference between the heterogeneous and homogeneous cases.

relatively stable across the entire range of electrode separations, with peak-to-peak voltages consistently in the range of approximately 230–250 μV. This indicates that the AE signal is largely insensitive to electrode spacing when electrodes are aligned with the ultrasound propagation direction.

In contrast, Scenario 4 shows a stronger dependence on electrode separation. The AE amplitude decreases rapidly as the separation increases, dropping from approximately 440 μV at the smallest separation to below 50 μV at 10 mm, and approaching zero for separations beyond 15 mm. This rapid decay indicates a significant loss of effective coupling between the acoustic pressure field and the electrical current distribution in the perpendicular configuration. Notably, the perpendicular configuration experiences a reduction of more than 90% in AE amplitude beyond 15 mm separation, whereas the parallel configuration maintains nearly constant signal levels, indicating significantly higher robustness to electrode spacing variations.

These results demonstrate that electrode orientation plays a dominant role over electrode separation in determining AE signal strength. When electrodes are aligned with the ultrasound propagation direction, the spatial overlap between acoustic pressure gradients and current density is preserved even at larger separations. However, when electrodes are arranged perpendicular to the propagation direction, increasing separation significantly reduces this overlap, leading to a substantial reduction in AE sensitivity.

While the simulations incorporate electrical heterogeneity through the inclusion model, several experimental non-idealities are not explicitly considered. In practice, acoustic attenuation and scattering in biological tissues will reduce the effective pressure amplitude, particularly at depth, leading to lower AE signal levels than those predicted in simulation. In addition, electrode–tissue interface impedance and contact variability may introduce measurement offsets and reduce sensitivity. Electrical noise from instrumentation, as well as motion artifacts, can further degrade the signal-to-noise ratio given the inherently weak nature of AE signals.

Moreover, acoustic and electrical property mismatches, as well as tissue anisotropy, may alter both the ultrasound field distribution and the resulting current density patterns. As a result, while absolute AE amplitudes may differ under experimental conditions, the relative trends observed in this study particularly the robustness of the parallel electrode

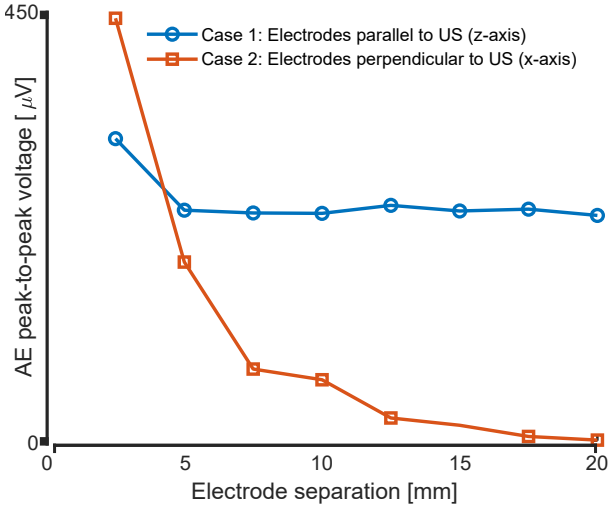

Fig. 4. Peak-to-peak voltage as a function of electrode separation distance in a homogeneous medium under focused ultrasound excitation. Scenario 3 (electrodes parallel to the ultrasound propagation direction) maintains a stable AE response of approximately 230–250 μV. In contrast, Scenario 4 (electrodes perpendicular to the propagation direction) exhibits a rapid decay in AE amplitude from approximately 440 μV at small separation to near zero at larger distances.

configuration and the rapid signal degradation in perpendicular configurations are expected to remain consistent. These findings therefore provide practical design guidance for real-world AET implementations.

Overall, the results suggest that, for minimal-electrode AET systems, alignment with the ultrasound propagation direction ensures robust AE signal generation, while perpendicular configurations require careful control of electrode spacing to avoid rapid signal degradation.

V. Conclusion

This work introduces a coupled 3D simulation framework for AET, integrating high-fidelity US field modelling (MUST) with finite-element bioimpedance analysis (EIDORS) to compute time-resolved AE voltages in homogeneous and heterogeneous media containing inclusions. The results show that AE sensitivity is governed by the spatial interplay between US field, electrode placement, and tissue conductivity: focused US generally provides higher AE amplitude and contrast than plane-wave excitation, electrode alignment with the US propagation direction maximizes the signal, and intralesional electrode placement yields substantially stronger and more robust contrast for both hypoconductive and hyperconductive inclusions than extracapsular placement. These findings establish a quantitative basis for optimizing US transmission (focused versus plane wave) and electrode configuration in minimal-electrode AET.

Additionally, we demonstrated that electrode separation has an impact on AE signal strength: while the AE response remains stable (approximately 230–250 μV) across a wide range of separations when electrodes are aligned with the ultrasound propagation direction, it rapidly decreases from approximately 440 μV to near zero for perpendicular configurations. This highlights the critical importance of electrode orientation in preserving AE sensitivity in minimal-electrode AET systems.

Together, these results establish a quantitative foundation for optimizing minimal AET system design and demonstrate the essential role of acoustic focusing in achieving high sensitivity with a limited number of electrodes. The coupled MUST–EIDORS framework provides a powerful tool for systematic exploration of electrode geometry, US field design, and measurement strategies prior to experimental implementation.

References

[1] H. Zhang *et al.*, "Biological current source imaging method based on acoustoelectric effect: A systematic review," *Frontiers in Neuroscience*, vol. 16, p. 807376, 2022.

[2] Y. Huang *et al.*, "Noninvasive visualization of electrical conductivity in tissues at the micrometer scale," *Science Advances*, vol. 7, no. 20, p. eabd1505, 2021.

[3] B. Lavandier, J. Jossinet, and D. Cathignol, "Experimental measurement of the acousto-electric interaction signal in saline solution," *Ultrasonics*, vol. 38, no. 9, pp. 929–936, 2000.

[4] G. Bal, "Inverse problems for acousto-electric tomography," *Inverse Problems*, vol. 26, no. 8, p. 085010, 2010.

[5] B. Jensen, A. Kirkeby, and K. Knudsen, "Feasibility of acousto-electric tomography," *Inverse Problems*, vol. 40, no. 7, p. 075007, 2024.

[6] R. Olafsson *et al.*, "Cardiac activation mapping using ultrasound current source density imaging (ucsdi)," *IEEE transactions on ultrasonics, ferroelectrics, and frequency control*, vol. 56, no. 3, pp. 565–574, 2009.

[7] G. Weinreich and H. G. White, "Observation of the acoustoelectric effect," *Physical Review*, vol. 106, no. 5, p. 1104, 1957.

[8] X. Li, R. Yang, J. Liu, and B. He, "Three-dimensional imaging of current density distribution using the acoustoelectric effect," *Physics in Medicine & Biology*, vol. 56, no. 13, pp. 3825–3840, 2011.

[9] T. L. Szabo, *Diagnostic Ultrasound Imaging: Inside Out*. Elsevier, 2004.

[10] Y. Zhou *et al.*, "Acoustoelectric brain imaging with different conductivities and acoustic distributions," *Frontiers in Physiology*, vol. 14, p. 1241640, 2023.

[11] M. Tanter and M. Fink, "Ultrafast imaging in biomedical ultrasound," *IEEE Transactions on Ultrasonics, Ferroelectrics, and Frequency Control*, vol. 49, no. 10, pp. 1363–1374, 2002.

[12] B. Keeshan, A. Adler, and C. Rossa, "Improved configurations for 3d acoustoelectric tomography with a minimal number of electrodes," *IEEE Transactions on Biomedical Engineering*, vol. 70, no. 12, pp. 3501–3512, 2023.

[13] B. Berthon *et al.*, "An integrated and highly sensitive ultrafast acoustoelectric imaging system for biomedical applications," *Physics in Medicine & Biology*, vol. 62, no. 14, p. 5808, 2017.

[14] R. Yang, X. Li, J. Liu, and B. He, "3d current source density imaging based on the acoustoelectric effect: a simulation study using unipolar pulses," *Physics in Medicine & Biology*, vol. 56, no. 13, p. 3825, 2011.

[15] P. Kuchment and L. Kunyansky, "2d and 3d reconstructions in acousto-electric tomography," *Inverse Problems*, vol. 27, no. 5, p. 055013, 2011.

[16] A. Cigier, F. Varray, and D. Garcia, "Simus: An open-source simulator for medical ultrasound imaging. part ii: Comparison with four simulators," *Computer Methods and Programs in Biomedicine*, vol. 220, p. 106774, 2022.

[17] D. Garcia and F. Varray, "Simus3: An open-source simulator for 3-d ultrasound imaging," *Computer Methods and Programs in Biomedicine*, vol. 250, p. 108169, 2024.

[18] A. Adler and W. R. Lionheart, "Uses and abuses of eidors: an extensible software base for eit," *Physiological measurement*, vol. 27, no. 5, p. S25, 2006.

[19] A. Adler and A. Boyle, "Electrical impedance tomography: Tissue properties to image measures," *IEEE Transactions on Biomedical Engineering*, vol. 64, no. 11, pp. 2494–2504, 2017.

[20] J. Jossinet and B. Lavandier, "The acoustoelectric effect in conducting liquids," *Ultrasonics*, vol. 36, no. 1-5, pp. 607–613, 1999.